Electronic Supplementary Information

Flexible strain sensors based on silver nanowires and UV-curable acrylate elastomers for wrist movement monitoring.

Shuhao Li[a], Wenjin Wu[a], Yu Chang[a], Weiquan Chen[a], Yijie Liu[a], Zifeng He[a], Yan Pu[a], Ivan S. Babichuk[a,b,*], Terry Tao Ye[c], Zhaoli Gao[d], and Jian Yang[a,*]

[a] *School of Mechanical and Automation Engineering and Jiangmen Key Laboratory of Intelligent Manufacturing of Polymer Materials, Wuyi University, Jiangmen 529020, Guangdong, P.R. China*
E-mail: jiany@szu.edu.cn

[b] *V. Lashkaryov Institute of Semiconductor Physics, NAS of Ukraine, Kyiv 03680, Ukraine*

[c] *Department of Electrical and Electronic Engineering and University Key Laboratory of Advanced Wireless Communications of Guangdong Province, Southern University of Science and Technology, Shenzhen, 518055, P.R. China*

[d] *Biomedical Engineering Department, The Chinese University of Hong Kong, Shatin, New Territories, Hong Kong, P.R. China; CUHK Shenzhen Research Institute, Nanshan, Shenzhen, 518060, P.R. China*

Material and methods

Materials and reagents

Silver nanowire dispersion (10 mg/ml AgNWs in bottle 50 ml, JCSW-995-70-45) was purchased from Nanjing Jichang Nanotechnology Co., LTD. Dodecyl acrylate (LA) and 4-hydroxybutyl acrylate (4-HBA) were purchased from Shanghai Aladdin Biochemical Technology Co., LTD. 2-hydroxy-2-methyl-1 phenylacetone (2-hydroxy-2-methylpropiophenone, photoinitiator 1173) was purchased from Ryoji. Polyvinyl alcohol (PVA, average molecular weight is 31000) was purchased from Guangzhou Haina Biotechnology Co., LTD. The conductive silver paste was purchased (3703, Shenzhen Xinwei Electronic Materials Co., LTD.). Additionally, polyethylene terephthalate (PET), fluorinated ethylene propylene (FEP), polyimide (PI), silicone plate, and deionized water (DI) were used.

Preparation of UV-curing flexible substrate films

Acrylate copolymer film was used as a substrate material for flexible strain sensors, as previously described.[1, 2] Two acrylate monomers, LA marked as L and 4-HBA as B, were mixed in different volume ratios of 6:4, 5:5, and 4:6, then added 1.5% volume of photoinitiator 1173, respectively. According to the volume proportion of LA and 4-HBA in their respective solutions, the solutions were named L4B6, L5B5, and L6B4. The mixed solution was injected into the mold with a silicone sheet and cured under 365 nm Ultraviolet (UV) light (365 nm, Shenzhen, China) with a light intensity of 18.5 mW/cm^2 for 30 s. After cooling, the film was taken, covered with FEP release films, and vacuumed for 12 h to obtain uniform acrylate copolymer elastomer films.

Fabrication of sensors

The glass slide was cleaned with ethanol and dried. After, the slide was put on a desktop homogenizing machine (KW-4N model, Institute of Microelectronics, Chinese Academy of Sciences) to spin-coating 200 μl of PVA/DI solution (60 mg/ml) for 15 s at a speed of

2000 r/min. Then, the coated spin-coated PVA slides were put into an oven (Binder, Germany) at 80 °C and dried for 3 min. The dried PVA films were used as the sacrifice layer of the flexible sensor. The acrylic copolymer elastomer film was made on this layer. By making the sensor substrate on the sacrificial layer, the sensor can be stripped on the slide without stress. The mask was used to make the electrode pattern using a laser processing process. The PET film (mask) with a size of 2.5 cm × 2 cm was cut and the pattern design was carried out using AutoCAD software. The designed pattern was imported into the laser processing platform BC-2902 (Beijing InitiaLase Technology Co., LTD., China), the laser is a 355 nm UV laser Grace X355-3a (Suzhou Yinggu Laser Co., LTD., China). The mask with the hollow-out electrode pattern was obtained by setting the cutting current to 7.5 A, the cutting speed to 6 mm/s, and 8 cutting times. The mask to the elastomer film was attached and evenly dropped 51 μl the AgNWs dispersion solution to the pattern (the concentration of AgNWs was 4 mg/ml (0.25 mg/cm^2)), placed at room temperature for 3 min, and then dried in the oven at 70 °C for 5 min. After drying, the mask was removed to obtain AgNWs@acrylate copolymer film with an electrode pattern. Five equal-length copper wires with the electrode pattern were placed on the film pins, and the copper wires were connected to the pattern with conductive silver paste. Finally, by curing a layer of UV solution on the electrode pattern for encapsulation, the strain sensor had better practicability and performance, and the encapsulated strain sensor was immersed in deionized water so that the sensor was detached from the slide without stress. The dried sensor was taken out and protected by PET release film. The effective area of the sensor was 12 mm × 20 mm, from whole size 20 mm × 25 mm.

Characterization structure of sensors

Infrared characterization and analysis of L6B4, L5B5 and L4B6 acrylate copolymer elastomer films were carried out by Fourier Transform Infrared Spectrometer (FTIR, Nicolet iS50, ThermoFisher Scientific Inc., USA). The attenuated total reflection (ATR) technique was

used. The scanning times were 50, the resolution was 16 cm^{-1}, and the test range was 4000 ~ 400 cm^{-1}. A dynamic testing machine (Fuletest Technology FLPL103E, Shanghai, China) was employed to stress-strain the L6B4, L5B5, and L4B6 film tests.[2] Using NOVA2S spectrometer and Gora ultralight system (ideaoptics, Shanghai, China /ideaoptics.com/) with Nd: YAG diode pumped solid state laser at 532 nm under the excitation of backscatter configuration of Raman spectra was investigation structure of sensors. A scanning electron microscope (SEM, Sigma 500, Zeiss, Germany) was used to observe the morphologies of acrylate films and AgNWs@acrylate copolymer films at a voltage of 15 kV. Uniaxial tensile experiments of three acrylate films were performed using a micromechanical test system (Fuletest Technology FLPL103E, Shanghai, China) with a stretching speed of 5 mm/s. The optical contact angle equipment (OCA25, DataPhysics Instruments GmbH, Filderstadt, Germany) was used to measure the acrylic film surface's water contact angle (hydrophilicity). The high-performance camera with up to 325 frames/s was used to receive optical photos. Deionized water was used for this measurement at the seat drop method with a droplet volume of 2 μl. Measurements were performed at 3 different points on the surface of each sample to get the average value.

Test of sensors

The electromechanical properties of three kinds of acrylic copolymer elastomer films were tested by a micromechanical testing system based on PT-SM40 (self-built in the laboratory).[1] The strain sensor was fixed on the electric slider (PT-SM40) with tape to test the tensile property of the sensor, and the resistance during tension was measured by a digital multimeter (KeySight-34465A, Keysight Technologies, UK). During the experiment, resistance values were collected at a fixed sampling rate of 500 ms. An NI data acquisition card (NI9205A, National Instruments Corp. UK) and a LabView program written by the laboratory were used to simultaneously record the resistance changes of each strain unit during wrist motion.

Performance analysis of flexible substrate films

Fig. S1(a) showed ATR FTIR spectra for three kinds of acrylate copolymer elastomers. The broadband, owing to its structures in the 3600–3150 cm^{-1} range, was representative of the O–H stretches of the synthesized compounds. The C–H stretch region (pprox. 3000–2800 cm^{-1}), which corresponds to methylene C–H asymmetric (ν_{as}) and symmetric (ν_{s}) stretches and in the fingerprint region between pprox. 1200–1000 cm^{-1} corresponds to C–O stretches of both ester and aliphatic ether functional groups. The aliphatic C–H vibrations were observed in the region of 2980–2850 cm^{-1} for LA and 4-HBA, as shown in Fig. S1(a). The intensity of the carbonyl stretches peak ν(C=O) at 1722±1 cm^{-1} in the spectra of LA and 4-HBA indicated the increased polymerization. The peak at 1633 cm^{-1} in the FTIR spectra of all UV curing films exhibited absorption due to ester carbonyl stretching vibration (C=C). It corresponded to the incorporation of the photoinitiator into the acrylate group. The asymmetric deformation ($\delta_{as}CH_3$) appeared near 1450±1 cm^{-1}. The absorption bands at 1396, 854 and 731 cm^{-1} were due to the bending of the C-H bond. The peak at 1251, 1163, 1058, 943 and 812 cm^{-1} were explained owing to the C–O–C, C–OH, C–OH_3 and C–C (ester bond) asymmetric stretching, bending and deformation vibration, respectively. Consequently, the influence of the different ratios of monomers on side chains, terminal end groups of long-chain molecules and functional groups was analyzed.

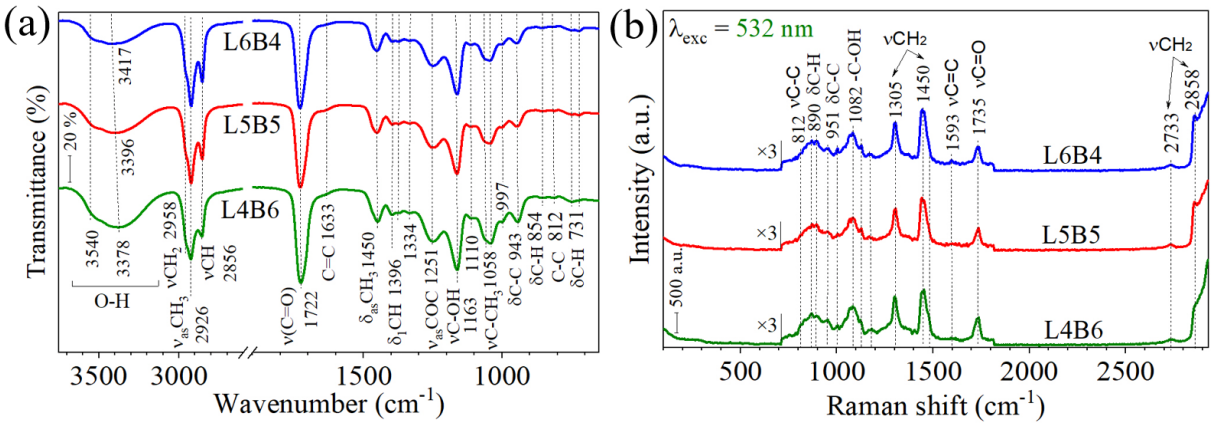

Fig. S1. (a) FTIR and (b) Raman spectra of acrylate copolymer films.

The Raman spectra (in Fig. S1(b)) show an intense band at high frequency. A band at 2858 cm^{-1} appears as a strong shoulder in the acrylate films and corresponds to ν_{as} asymmetric vibration of the methylene group, $\nu_{as}(CH_2)$. The shoulder strengthens as the concentration of lauryl acrylate (LA) increases. In contrast, a weak band (2733 cm^{-1}) for the symmetric stretching of a methylene group, $\nu_a(CH_2)$ is observed in all bands. The band at 1735 cm^{-1} corresponds to the carbonyl stretching mode ν(C=O). Weak bands located at 1593 and 812 cm^{-1} correspond ν(C=C) and ν(C–C) stretching modes for the acrylate films.[3] The weak shoulder at 1480 cm^{-1} is near the strong band at 1450 cm^{-1}, and the band at 890 cm^{-1} corresponds to methylene bending $\delta(CH_2)$. The vibrations of bands at 1450 and 1305 cm^{-1} correspond $\nu(CH_2)$ stretching modes. Also, the band at 1082 cm^{-1} corresponds to –C–OH vibration. The weak band at 951 cm^{-1} corresponds to δ(C–C) bending mode.[4]

Thus, structural studies have shown the quality of bonds formed in acrylate copolymer elastomers. Band shifting was not observed when the ratio of film components was changed, while the concentration-dependent intensity clearly shows the correlation between the intensity of the bands and the change in the ratio of copolymer components.

The findings, presented in Fig. S2, supplement the data in Fig. 2(c and d) and offer a systematic analysis of the mechanical properties associated with sensor sensitivity.

An increase in the level of the L component in the acrylic solution (L:B) leads to a decrease in the elastic modulus (Young's modulus) in the resulting UV-cured film (Fig. 2(c)), which is reflected in a more hydrophobic surface due to an increased contact angle (Fig. 2(d)). The plastic deformation in the acrylic solution is influenced by the proportion of B, as indicated in this study. The elastomers exhibit a high strain of approximately 481% (Fig. S2(a)) when the proportion of B is 50% and visibly grows with the increase in the level of B. The breaking test (Fig. S2(b)) and the elastic modulus (Fig. 2(c)) also demonstrate the same trend. However, no significant changes were observed if the proportion of B was further increased.

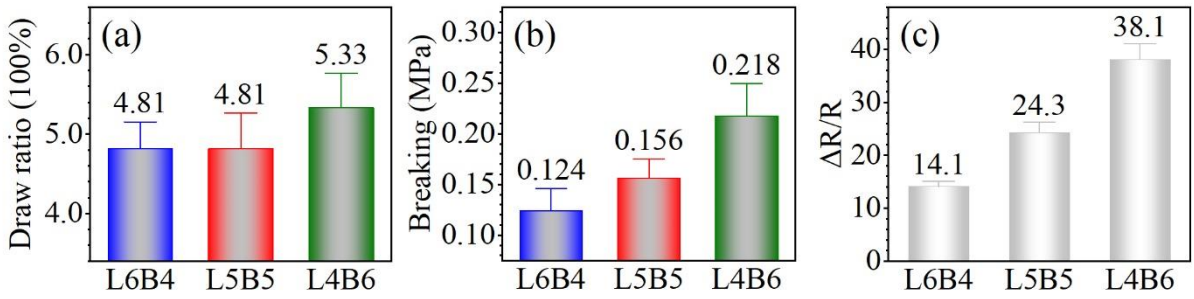

Fig. S2. Uniaxial tensile stress-strain analysis for acrylate substrates: (a) Draw ratio and (b) Breaking. (c) Relative resistance for sensors with different substrates at maximum strain (Table S2).

Therefore, a preferred interaction between the substrate and the nanomaterial can be realized with a reduced hydrophobicity. That is, a lower hydrophobicity is inversely related to adhesion. The elastic modulus for L4B6 (38.6 kPa) is close to human skin (Young's modulus of about 50 kPa[5]) and with good adhesion, in this case, for the interaction between the sensor and the skin on the wrist, allowing an increase in the sensitivity of the flexible device. So, considering that and the results shown in Fig. S2(c), flexible strain sensors should be manufactured based on the L4B6 substrate.

Strain analysis of the L4B6 acrylate copolymer film and AgNWs

The SEM surface morphology of acrylate copolymer substrate (L4B6) and AgNWs on this film at varied stretching is shown in Fig. 3(c). Subtle folds were observed on the surface of the L4B6 acrylate copolymer film, stretching from 0% to 30%. Their density increased with tensile strain (inserts SEM photos). In the strain sensor (AgNWs@L4B6), during stretching from 0% to 30%, cracks and their gradual enlargement with increased tension in conductive electrodes were observed. The folds were also discovered, where AgNWs were pushing on each other due to the narrowing of the substrate in the perpendicular direction to the tensile direction.

Also, the folds can be caused by substrate shrinkage due to the positive Poisson's ratio of acrylate elastomer ($\approx$ 0.3). Poisson's ratio is the ratio of transverse contraction strain (ε_{trans}) to longitudinal extension, strain ($\varepsilon_{longitudinal}$) in the direction of stretching force. Tensile deformation is considered positive, and compressive deformation is negative. The definition of Poisson's ratio contains a minus sign so that regular materials have a positive ratio ($\nu = -\varepsilon_{trans}/\varepsilon_{longitudinal}$).[6] Strain ($\varepsilon$) is defined in elementary form as the change in length (ΔL) divided by the original length (L_0): $\varepsilon = \Delta L/L_0$.[7]

The inserts in SEM photos (Fig. 3(c)) showed AgNWs@L4B6 sensors at higher magnifications: conductive film, cross-section in 45° oblique plane, from which was confirmed that AgNWs are uniformly distributed on the surface of the L4B6 film and its sizes (diameter 70 nm, length about ~1-10 μm) and cracks. The width of those cracks increased proportionally with the rise in tension. In addition, part of the AgNWs length was wrapped by the L4B6 elastomer film because the acrylate elastomer has a good elasticity of stretching and viscosity,[2] which should contribute to the stability of the sensors' resistance in cyclic stretching many times. The high viscosity of the acrylic film may have a partial effect on the appearance of wrinkles in the conductive layer. Consequently, in our case, as Ref.[8] shows that cracks in the electrodes generated during uniaxial stretching are the main reason for decreased conductive paths and increased resistance. In contrast, the effect of folds in the substrate and electrodes on the resistance change is insignificant.

The Raman spectra (Fig. S3) show an intense polyvinyl pyrrolidone (PVP)[9] band and a low-intense band of the AgNWs. The use of insulating PVP surfactant limits the conductivity of the final AgNWs networks (PVP used in the formation of AgNWs[10]). The bands 221 cm^{-1} correspond to the vibration of Ag–O stretching. The absence of a band shift can be interpreted as the sliding of the nanowires relatively uniform and relative to the substrate due to the absence of tensile or compressive stress of the Ag–O band.

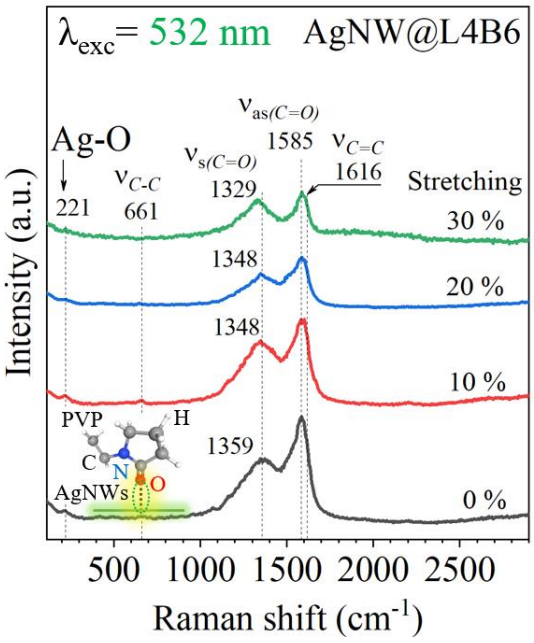

Fig. S3. Raman spectra AgNWs on L4B6 flexible substrate at varied stretching. Schematic illustration of PVP conformation on the surface of Ag nanowires (insert).

A decrease in intensity is visible, which corresponds to a reduction in the concentration of nanowires due to spreading over a larger area due to the stretching of the substrate. The bands at 1359 and 1585 cm^{-1} are obtained due to the carboxylic symmetric and anti-symmetric C=O stretching vibration of the carboxylic group,[11] respectively. The significantly enhanced Raman bands indicate that PVP molecules interact mainly with silver nanowires through oxygen (Fig. S3, insert).[12] The 661 and 1616 cm^{-1} bands correspond to C–C and C=C stretching modes for PVP, respectively.[3] One extremity of the oxidized PVP is linked to the polymer via an ester bond, hydrogen bond, and various forces, while the other extremity forms a bond with the AgNWs through an Ag–O bond. Thus, it was additionally confirmed that AgNWs don't undergo significant changes during stretching, and only the intensity of the Ag–O band decreases, corresponding to a reduction in the concentration of the conductive layer. Therefore, the main changes in conductivity can be evident only due to the properties of acrylic films, which could fix the nanowires on their surface and distribute them during stretching.

To identify additional strain-induced mechanisms that affect the change in resistance additional investigations were conducted. The effect of various strain directions on the deformation (stress) of the AgNWs pattern was analyzed qualitatively using finite element method (FEM) in ANSYS 19.0® software. Fig. S4(a) shows a portion of each strain unit, with a length of 4.25 mm and a width of 1.5 mm. The complete length of each unit can be found in Table S1.

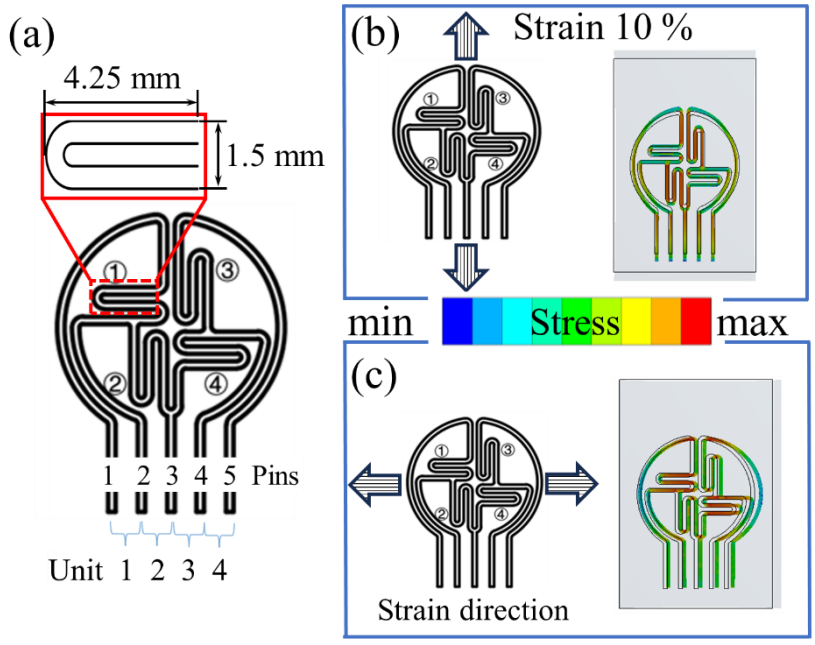

Fig. S4. (a) The sensor structure and dimensions of each unit (b) Representative of the FEM simulations under parallel (b) and perpendicular (c) strain direction to AgNWs pins electrodes.

According to the simulation results of the FEM, when the sensor is stretched by 10% along the direction of the pin electrodes, the stress is primarily concentrated in units 2 and 3, which are parallel to the direction of motion (Fig. S4(b)). On the other hand, the stress in units 1 and 4, which are perpendicular to the direction of motion, is significantly reduced. Likewise, when the sensor is stretched perpendicular to the pin AgNWs electrodes, the differences in stress between strain units 1 and 4 will be more pronounced compared to the differences in strain units 2 and 3 (Fig. S4(c)). At the same time, the stress on the straight part of units is more significant

than the stress on the curved. This correlates with the experimental data in Figs. 4(b) and (c), where higher piezoresistive sensitivity was observed for units with the same direction as the strain direction. Another observation from the simulation of the FEM indicates that the strain in the direction parallel to the pin electrodes is greater, as evidenced by the $\Delta R/R_0$ value of 0.8 (Fig. 4(b)), compared to the value of 0.15 (Fig. 4(c)) in the perpendicular direction.

Therefore, the innovative substrate and cost-effective design of the suggested sensor enabled the demonstration of sensitivity distribution in the piezoresistive device. These sensitive sensors can better recognize human movements, which will help people with increased support services and analyze their health conditions.

Comparison of elongation at break and strength for AgNWs@L4B6 strain sensor with different AgNWs concentrations shown in Fig S5.

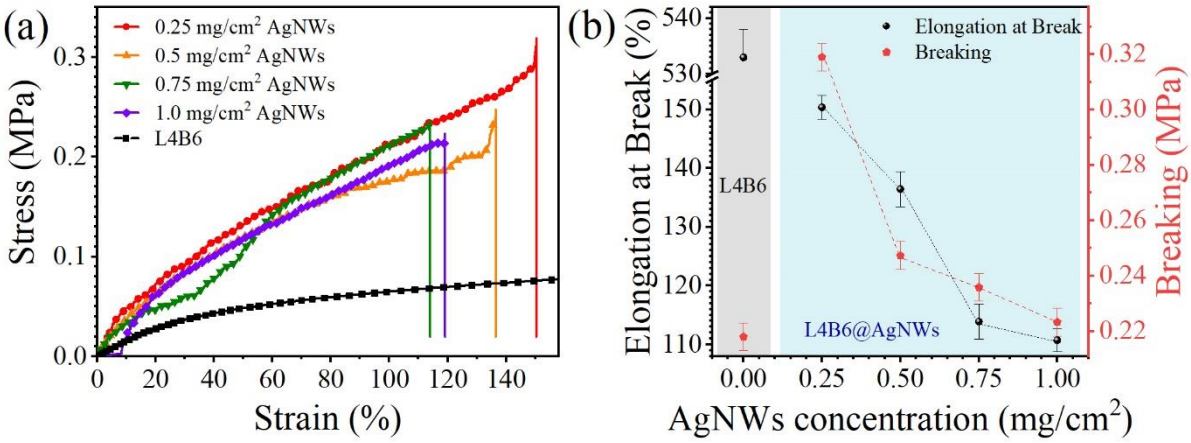

Fig. S5. (a) Stress-strain curves of AgNWs@L4B6 strain sensor with different AgNWs concentrations and their comparison of elongation at break and strength (b).

A dynamic and static fatigue test system (Fuletest Technology FLPL103E, Shanghai, China) was employed to better analyze the mechanical properties of the AgNWs@L4B6 strain sensors with different AgNWs concentrations. The mechanical properties were compared to those exhibited by pure L4B6 film. Based on Fig. S2, Fig. 2(c) and Fig. S5 provided, it is evident that the pure L4B6 film exhibits an elongation at a break of 533% and a breaking strength of

0.218 MPa. Fig. S5(a) and analysis in Fig. S5(b) shows, that with a solution AgNWs deposited to the surface at a content of 0.25 mg/cm^2, there was a significant change in the relative elongation at break (150.4%), but the fracture strength reaches its highest point at 0.319 MPa. As the concentration increased to 0.5 mg/cm^2, both the elongation at break and the fracture strength decreased by 136.4% and 0.247 MPa, respectively. A subsequent increase in concentration, there was a consistent decline in both the elongation at break and the tensile strength at break.

Fig. S6 shows the measurements between pins 1 and 5 which includes all the resistors, specifically, Units 1-4 to prove the feasibility of our development design (Fig. 4 and Fig. S4).

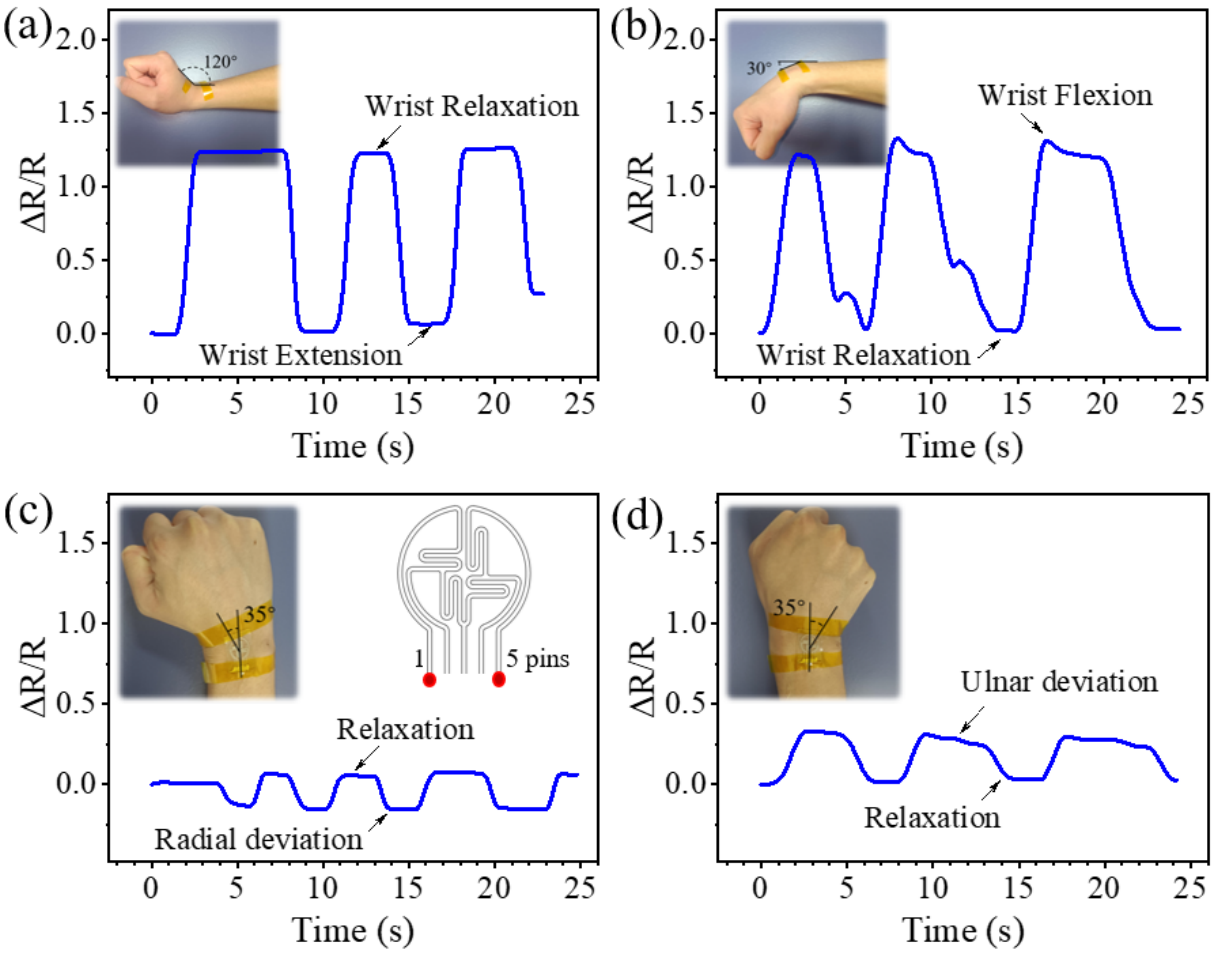

Fig. S6. Total relative resistance changes of the sensor during wrist movement for an extension on 120° (a), bending on 30° (b), radial (c) and ulnar (d) deviations on 35°, respectively, with three cycles for each angle.

The normalized resistance change ($\Delta R/R_0$) during the wrist flexion motion) increased with the degree of bending and the wrist extension motion decreased with compression (Fig. S6). Note, in the wrist extension movement, the resistance changes of unit 3 and unit 1 were more evident than the resistance changes of unit 4 and unit 2 (Fig. 4(d and e)) and the radial movement, unit 1 and unit 2 were changed more obviously than unit 3 and unit 4 (Fig. 4(f and g)). So, relative to the wrist bending (flexion) action, the change of the strain sensor in the ulnar and radial deviation of the wrist is relatively complex.

Table S1. Parameters of each unit in the sensor and their corresponding resistances.

Connection pins	Length (mm)	Height (mm)	Width (mm)	Area (mm^2)	R_{calc} (Ω)	R_{measur} (Ω)
1-2	59.9				9.0	21.8
1-3	63.1				9.5	22.8
2-3	36.0				5.4	14.6
3-4	38.2	0.00021	0.5	0.00015	5.7	15.5
4-5	52.7				7.9	23.9
3-5	64.2				9.7	25.5
1-5	114.7				17.3	40.4

Table 1 shows the relative values of the length of each sensor element and the corresponding values of the resistance of each section without stretching. Table S1 also shows a comparison between the measured resistance value and the one calculated using Eq. S1.[13]

$$R_{calc} = \rho \frac{L}{A} \quad \text{(S1)}$$

where R_{calc} corresponds to the calculation resistance, L is the original length of each unit in the sensor, A – a cross-section of AgNWs electrode and ρ is the resistivity of 1 m of the AgNWs in Ω×m. To calculate the resistance of each sensor element, it was used the value of the resistivity of silver was $\rho = 1.59\times10^{-8}$ Ω×m. In Ref.[14] the sensitivity of the strain sensors to stretching depends on the AgNWs concentration in the solution. Even though this work used a higher resistivity value than that reported in the literature for AgNWs, the actual resistance R_{measur} values were still higher than the calculated ones R_{calc}. This shows that additional factors need

to be further studied. The authors suggest that one factor increasing the natural resistance could be the solution (PVP) in which the AgNWs were kept before drying on the substrate.

In practical applications, the relative change in resistance during tensile tests for strain sensors can help understand the performance characteristics of the sensors, including their sensitivity, linearity, stability, and so on. Meanwhile, the tensile strain test can also calibrate the strain sensors to improve their accuracy and reliability to meet the requirements of different application scenarios. From Fig. 3(a), it can be discovered that when the strain range is between 0% and 10%, the resistance and the rate of change resistance do not fluctuate much, showing a relatively stable upward trend. The number of cracks in the conductive film increases uniformly at this stage (see Fig. 3(c)). In the strain range between 10 % and 30 %, the resistance change rate was raised significantly, mainly dependent on the cracks on the surface of the thin conductive film of the AgNWs, which gradually widened and increased. The number of contact junctions in AgNWs was reduced, rapidly reducing the conductive path. In this strain range for AgNWs@L5B5 and AgNWs@L6B4 sensors, the resistance and the rate of change of the resistance rise rapidly, and the interaction between the AgNWs and the acrylate polymer matrix undergoes a significant change. The same situation was observed for the AgNWs@L4B6 sensor, although in the higher strain range of 35%~50%.

GF can be quantitatively expressed as the ratio of the relative change in resistance to the strain. The sensitivity of strain sensors prepared with different conductive materials and polymer matrix materials depends mainly on factors such as the sensor's structure and the conductive network's design.[15] Typically, the higher the strain sensitivity factor GF of the sensor, the more it can detect minor strain signals with higher accuracy. Therefore, the sensor's sensitivity is one of the important parameters that determine whether the sensor can detect the subtle movements of the human body. In our case, sensors based on AgNWs@L5B5 and AgNWs@L6B4 have higher strain sensitivity factors GF = 97 and GF = 70, respectively.

However, their use is limited to a stretch range of up to 25% and the lowest parameter of linearity R^2, so wrist movement monitoring was shown for AgNWs@L4B6 sensor with sensitivity GF = 58 at strain 68% and R^2 ~ 98. Compared to some reported flexible strain sensors (Table S2), the strain sensors in this work exhibited good sensitivities at maximum strain due to the innovation of UV-curable substrates.

Table S2. Comparison of flexible strain sensors.

Compound of sensor	Maximum strain (%)	GF (tension)	Cycles (tension)	References
PDMS@AgNWs	35	20 (35%)	1000 (0~10%)	[16]
PDMS@AgNWs	20	14.3 (15%)	8000 (0~15%)	[17]
PDMS@AgNWs-Acrylate	50	104-86 (8%)	7500 (0~1.5%)	[18]
Silicone sheets@AgNWs-PEO	50	100 (50%)	N/A	[14]
PDMS@AgNWs-CNT	50	6.7 (50%)	1000 (0~30%)	[19]
POC-PEG@AgNWs CPES	50	231.6 (50%)	800 (0~25%)	[20]
TPU@AgNWs	240	12.65 (240%)	2000 (0~15%)	[21]
PUU@AgNWs@PDMS	100	30 (100%)	2500 (0~100%)	[22]
TPU@AgNWs	85	337 (85%)	200 (0~10%)	[23]
L4B6@AgNWs	68	58 (68%)	200 (0~10%)	
L5B5@AgNWs	24	97 (24%)	200 (0~10%)	this work
L6B4@AgNWs	19	70 (19%)	200 (0~10%)	

The stability investigation showed good sensitivity of the sensor during 200 stretching/releasing cycles. This demonstrates that such a sensor can effectively monitor human movements.

It was shown that the direction of stretching has a significant response in changing the relative resistance $\Delta R/R_0$ of the sensor depending on the design of its contact grid, so the development and implementation of innovative design solutions remain open.

Overall, it can be concluded that despite performance and advancement issues such as roughness, structure and performance stability, high cost, and low abundance, the scalable utilization of these nanowires in the industry still hinders. Unlike nanowires, the proposed innovative substrate has all the chances to be used to manufacture sensors based on it on an industrial scale.

References

1. W. Chen, Y. Qiu, I. S. Babichuk, Y. Chang, R. Zhou, Z. He, Y. Liu, J. Zhang, I. V. Babichuk, A. Tiutiunnyk, D. Laroze, V. V. Brus and J. Yang, *Adv. Eng. Mater.*, 2023, **26**, 2301470.
2. C. Lin, W. Wu, H. Zhu, Y. Qiu, S. Cui, W. Chen, I. S. Babichuk, T. T. Ye, Z. Gao and J. Yang, *Adv. Mater. Technol.*, 2023, **8**, 2202142.
3. F. J. Boerio, S. K. Bahl and G. E. McGraw, *J. Polym. Sci. B Polym. Phys.*, 2003, **14**, 1029-1046.
4. M. Olivares, A. Alvarez-Castillo, J. P. Molina, M. Corea-Téllez, F. Vázquez, B. Lizama and V. M. Castaño, *Int. J. Polym. Mater.*, 2004, **53**, 395-404.
5. A. Kalra, A. Lowe and A. M. Al-Jumaily, *J. Material. Sci. Eng.*, 2016, **5**, 1000254.
6. J. Karpiesiuk, *Mod. App. Matrl. Sci.*, 2020, **2**, 251-255.
7. X. Wang, H. Li, T. Wang, X. Niu, Y. Wang, S. Xu, Y. Jiang, L. Chen and H. Liu, *RSC Adv.*, 2022, **12**, 14190-14196.
8. Y. Heo, Y. Hwang, H. S. Jung, S. H. Choa and H. C. Ko, *Small*, 2017, **13**.
9. R. Yin, S. Yang, Q. Li, S. Zhang, H. Liu, J. Han, C. Liu and C. Shen, *Sci. Bull.*, 2020, **65**, 899-908.
10. F. Zhang, B. Cheng, J. Liu, Y. Yue, Z. Huang, Y. Zhang and D. Zang, *J. Mater. Res. Technol.*, 2020, **9**, 14509-14516.
11. Y. Shen, W. Yang, F. Hu, X. Zheng, Y. Zheng, H. Liu, H. Algadi and K. Chen, *Adv. Compos. Hybrid. Mater.*, 2022, **6**, 1-11.
12. H. Mao, J. Feng, X. Ma, C. Wu and X. Zhao, *J. Nanopart. Res.*, 2012, **14**.
13. R. A. Matula, *J. Phys. Chem. Ref. Data*, 1979, **8**, 1147-1298.
14. H.-C. Lu and Y.-C. Liao, *Nanomaterials*, 2021, **11**, 2583.
15. L. Duan, D. R. D'Hooge and L. Cardon, *Prog. Mater. Sci.*, 2020, **114**, 100617.
16. K. K. Kim, S. Hong, H. M. Cho, J. Lee, Y. D. Suh, J. Ham and S. H. Ko, *Nano Lett.*, 2015, **15**, 5240-5247.
17. W. Zhou, Y. Li, P. Li, J. Chen, R. Xu, S. Yao, Z. Cui, R. Booth, B. Mi, D. Wang, Y. Ma and W. Huang, *Adv. Mater. Technol.*, 2019, **4**, 1800698.
18. G.-S. Liu, F. Yang, J. Xu, Y. Kong, H. Zheng, L. Chen, Y. Chen, M. X. Wu, B.-R. Yang, Y. Luo and Z. Chen, *ACS Appl. Mater. Interfaces*, 2020, **12**, 47729-47738.
19. M.-Y. Liu, C.-Z. Hang, X.-Y. Wu, L.-Y. Zhu, X.-H. Wen, Y. Wang, X.-F. Zhao and H.-L. Lu, *Nanotechnology*, 2022, **33**, 255501.
20. Z. Wang, H. Zhou, B. Zheng, Y. Gao, H. Zhang, X. Jin, G. Zhang and A. Ma, *Soft Science*, 2022, **2**, 16.
21. L. Zhang, F. Jiang, L. Wang, Y. Feng, D. Yu, T. Yang, M. Wu and M. Petru, *Appl. Compos. Mater.*, 2022, **29**, 1621-1636.
22. C.-J. Lee, K. H. Park, C. J. Han, M. S. Oh, B. You, Y.-S. Kim and J.-W. Kim, *Sci. Rep.*, 2017, **7**, 7959.
23. R. Wang, W. Xu, W. Shen, X. Shi, J. Huang and W. Song, *Inorg. Chem. Front.*, 2019, **6**, 3119-3124.